Cell Reports
Physical Science

Article

Isolation of elusive gold-phosphane tellurides: From bonding to σ-hole dynamics

Graphical abstract

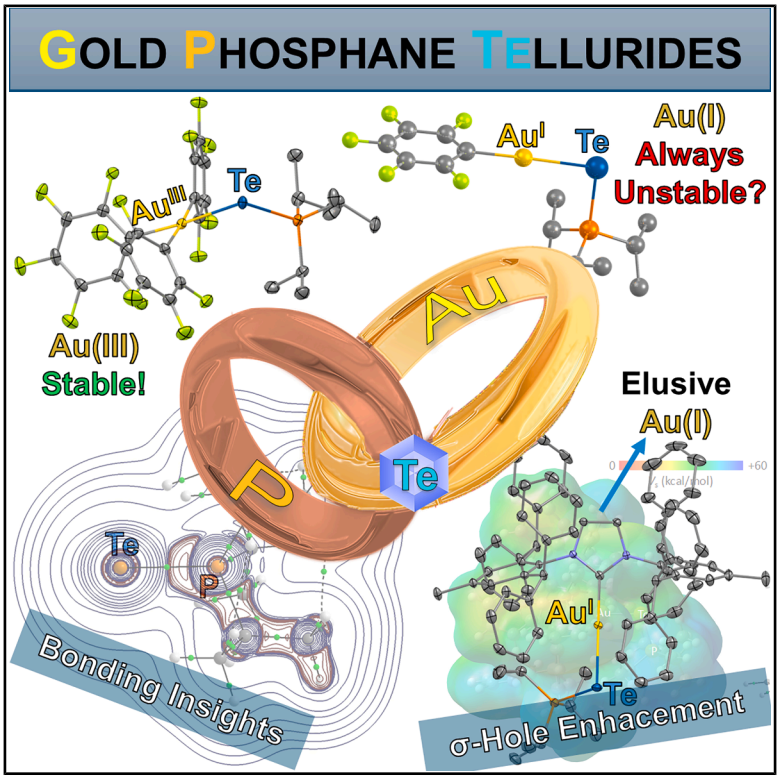

Highlights

- Gold(III) phosphane tellurides show superior stability over gold(I) analogs
- Steric design enables isolation of elusive gold(I) phosphane telluride complexes
- Gold coordination amplifies Te σ-hole, enabling chalcogen bond catalysis
- Bonding in phosphane chalcogenides revisited through DFT and IQA analyses

Authors

Juan Carlos Pérez-Sánchez, Carmen Ceamanos, Jorge Echeverría, Juan V. Alegre-Requena, Raquel P. Herrera, M. Concepción Gimeno

Correspondence

gimeno@unizar.es

In brief

Pérez-Sánchez et al. isolate unstable gold-phosphane tellurides and uncover how gold coordination amplifies tellurium's σ-hole, enhancing its reactivity. Their findings bridge bonding fundamentals and chalcogen bonding catalysis, revealing how subtle changes in structure and electronics control complex stability and tellurium transfer pathways.

Pérez-Sánchez et al., 2025, Cell Reports Physical Science 6, 102717
August 20, 2025
https://doi.org/10.1016/j.xcrp.2025.102717

CellPress

Please cite this article in press as: Pérez-Sánchez et al., Isolation of elusive gold-phosphane tellurides: From bonding to σ-hole dynamics, Cell Reports Physical Science (2025), https://doi.org/10.1016/j.xcrp.2025.102717

Cell Reports
Physical Science

CellPress
OPEN ACCESS

Article

Isolation of elusive gold-phosphane tellurides: From bonding to σ-hole dynamics

Juan Carlos Pérez-Sánchez,[1,2] Carmen Ceamanos,[1] Jorge Echeverría,[1] Juan V. Alegre-Requena,[1] Raquel P. Herrera,[2] and M. Concepción Gimeno[1,3,*]

[1]Departamento de Química Inorgánica, Instituto de Síntesis Química y Catálisis Homogénea (ISQCH) CSIC-Universidad de Zaragoza, Pedro Cerbuna 12, 50009 Zaragoza, Spain

[2]Laboratorio de Organocatálisis Asimétrica, Departamento de Química Orgánica, Instituto de Síntesis Química y Catálisis Homogénea (ISQCH) CSIC-Universidad de Zaragoza, Pedro Cerbuna 12, 50009 Zaragoza, Spain

[3]Lead contact

*Correspondence: gimeno@unizar.es

https://doi.org/10.1016/j.xcrp.2025.102717

SUMMARY

Tellurium, one of Earth's rarest elements, plays a crucial role in electronic and materials applications, yet its coordination chemistry with metals remains underexplored. Although gold and tellurium coexist in nature, their chemical interactions and tellurium transfer processes between metals are poorly understood due to the instability of intermediates. Here, we report the synthesis of elusive gold(I) and gold(III) complexes featuring a terminal triisopropylphosphane telluride, representing snapshots of a phosphane-mediated tellurium transfer. In gold(I) species, this process is driven by intermolecular Au···Au interactions, leading to decomposition. This instability is overcome by using a sterically demanding N-heterocyclic carbene, enabling the isolation of the first gold(I) complex with a terminal (^{i}Pr)$_3$PTe ligand. Spectroscopic and computational studies reveal unique bonding trends across the chalcogen series (O, S, Se, and Te) and demonstrate that gold coordination amplifies the tellurium σ-hole, enhancing chalcogen bond catalysis, with the cationic gold(I) complex as the most active catalyst.

INTRODUCTION

Tellurium has emerged as a critical element with a diverse range of applications, including its role in specialized alloys for thermoelectric cooling devices,[1] photovoltaic solar cells,[2] and semiconductor materials[3] (Figure 1A). Furthermore, advancements in medical applications have highlighted the significance of tellurium compounds despite the absence of a known biological role, unlike selenium.[4] Notably, tellurium derivatives exhibit antitumoral, immunomodulatory, and neuroprotective properties, primarily attributed to their ability to inhibit cysteine proteases and their selenium-like antioxidant activity (Figure 1A).[5] The growing impact of tellurium compounds[6] is further underscored by the recent emergence of chalcogen bonding (ChB).[7–9] Contrasting halogens, chalcogen atoms possess two σ-holes, facilitating multiple ChB interactions wherein the chalcogen atom can function both as a Lewis acid by utilizing its σ-holes and as a Lewis base by using its lone pairs. This unique property has found applications in crystal engineering,[10] anion recognition,[11] and catalysis,[12] with ChB-driven organocatalysis showing promise (Figure 1A).[13] Despite these advancements, tellurium remains a "*rara avis*," as its behavior notably deviates from that of its congeners.

Phosphane chalcogenides, R$_3$P=E (E = O, S, Se, or Te; R = alkyl or aryl), exemplify the versatile chemistry of group 16 elements (Figure 1B).[18] These compounds are notable for their diverse electronic and chemical properties (Figure 1B),[19] oxidation states,[20] and chalcogen-chalcogen interactions,[21] with their Lewis base character transitioning from hard to soft across the group. The bonding in phosphane chalcogenides, traditionally depicted as a double bond, has been a topic of significant debate, especially for elements from the third period and beyond.[22] Resonance structures, ranging from a double P=E (**I**; Figure 1B) bond to a polarized single P$^+$–E$^-$ bond (**II**; Figure 1B), provide a reasonable depiction of the bonding nature and behavior of these compounds. Consequently, the hitherto P=E formulation oversimplifies the bonding, especially given the variations between lighter and heavier chalcogens. Despite these advances, the synthesis of phosphane telluride complexes remains a significant challenge, restricting further exploration of their chemical and coordination properties.

While phosphane oxides, sulfides, and selenides have been extensively studied,[23,24] the coordination chemistry of phosphane tellurides remains an underexplored field. Kuhn's seminal work in 1985 on M(CO)$_5$(TeP^{t}Bu$_3$) (M = Cr, Mo, or W) complexes (**a**; Figure 1C)[14] paved the way for the coordination chemistry of phosphane tellurides, demonstrating their potential as ligands. However, progress since then has been limited, primarily due to the thermal and photochemical instability of these compounds, which complicates their synthesis. Subsequent studies included the synthesis of a (η^5-C$_5$H$_5$) piano-stool iron(II) complex (**b**; Figure 1C)[15] and scarce silver(I) complexes featuring the

CellPress
OPEN ACCESS

Cell Reports
Physical Science
Article

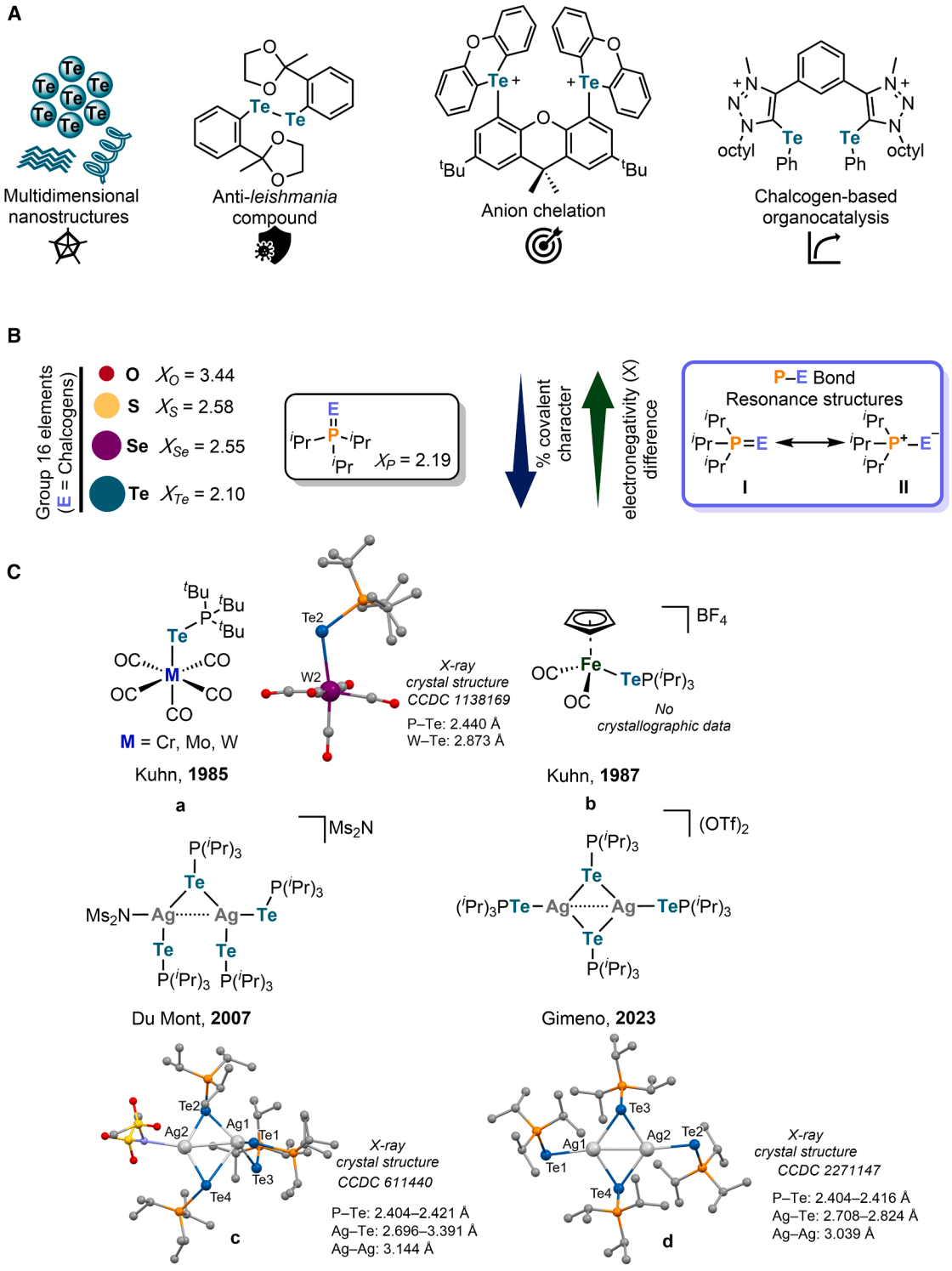

Figure 1. Properties of chalcogen group phosphanes and the representation of tellurium in diverse compounds

(A) Selected examples of tellurium element in multiple applications. X-ray structures adapted from the corresponding data deposited at CCDC,[14–17] counterions, and hydrogen atoms have been omitted for clarity.

(B) Periodic trends across group 16 phosphanes and resonant forms.

(C) Selected examples of isolated metal complexes bearing R_3PTe (R = ^{t}Bu or ^{i}Pr) as ligand.

Please cite this article in press as: Pérez-Sánchez et al., Isolation of elusive gold-phosphane tellurides: From bonding to σ-hole dynamics, Cell Reports Physical Science (2025), https://doi.org/10.1016/j.xcrp.2025.102717

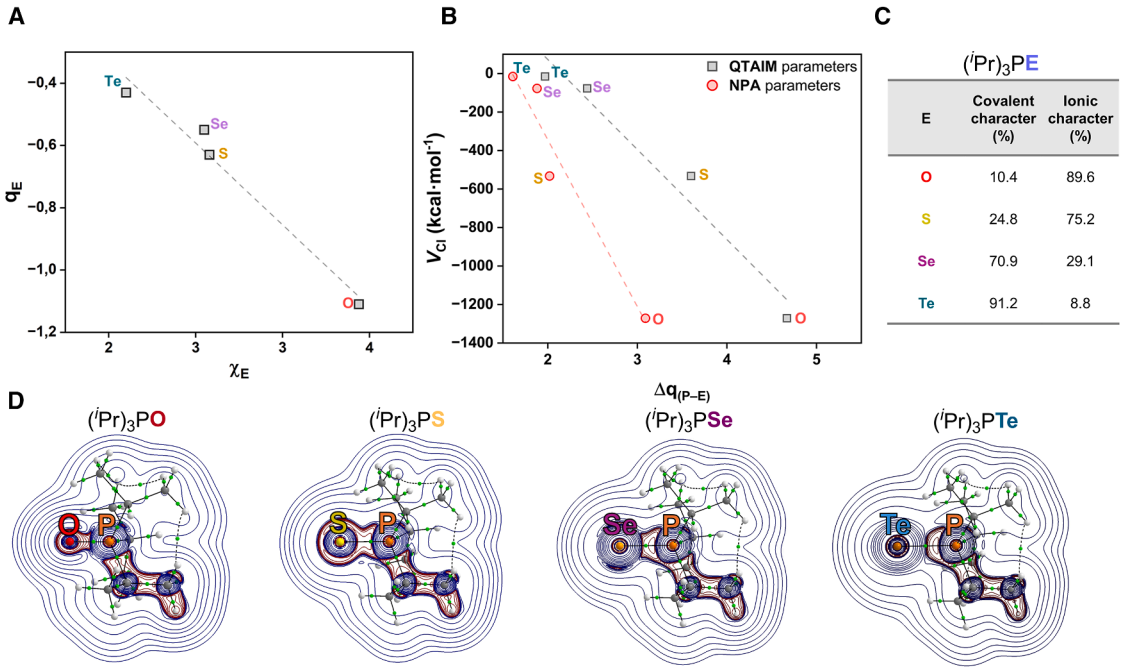

Figure 2. Theoretical calculations on the bonding nature of phosphane chalcogenides

(A) Relationship between the atomic charge of E and its corresponding Pauling electronegativity value.

(B) Linear correlations between the NPA (red circles) and QTAIM (gray squares) atomic charge differences and the value of V_{Cl} for (^{i}Pr)$_3$P=E.

(C) Degree of covalency and ionicity of P=E bonds in (^{i}Pr)$_3$P=E molecules according to IQA analysis.

(D) View of the P–E interaction in phosphane chalcogenides, displaying the Laplacian of the electron density (QTAIM analysis), bond paths, and bond critical points.

(^{i}Pr)$_3$PTe ligand in both the terminal and bridging coordination modes (**c** and **d**; Figure 1C).[16,17] Despite these advances, the synthesis of phosphane telluride complexes remains a significant challenge, restricting further exploration of their chemical and coordination properties.

Regarding this matter, group 11 metals, particularly gold, display a strong affinity for sulfur and selenium, leading to numerous applications of this gold-chalcogen binomial in catalysis,[25] luminescence,[26] and medicinal chemistry.[27] Despite the presence of tellurium in gold-containing minerals such as calaverite and krennerite ($AuTe_2$),[28] the synthesis and structural characterization of gold-tellurium complexes are significantly less developed compared to their sulfur and selenium analogs. This knowledge gap limits the rational design of functional tellurium-based materials and catalysts, impeding innovation in fields that rely on precise control over heavy-element behavior. This work addresses this challenge by exploring phosphane tellurides as molecular tools to access and manipulate gold-tellurium interactions, which are naturally occurring but chemically underexplored. Herein, we report the synthesis, structural characterization, and bonding analysis of gold(I) and gold(III) complexes bearing the triisopropylphosphane telluride ligand, (^{i}Pr)$_3$PTe. Significant advances include the first isolation of a gold(I) phosphane telluride complex, stabilized by a sterically hindered N-heterocyclic carbene, and the finding that gold coordination significantly amplifies the tellurium σ-hole, unlocking innovative potential in ChB activation.

RESULTS AND DISCUSSION

Computational study of the phosphorus-chalcogen bond in triisopropylphosphanes

As previously discussed, bonding in phosphane chalcogenides has traditionally been explained in terms of two resonance forms: an uncharged structure **I** (Figure 1B) involving a double bond between the phosphorus and chalcogen atoms and a zwitterionic structure **II** (Figure 1B) featuring a P^+–E$^-$ single bond with positive and negative formal charges on the phosphorus and the chalcogen atoms, respectively. By means of NPA (natural population analysis) and QTAIM (quantum theory of atoms in molecules) calculations,[29,30] we have studied here the nature of the phosphorus-chalcogen bond in (^{i}Pr)$_3$P=E (E = O, S, Se, or Te) molecules (Figure 2). After full geometry optimization, an NPA was run (Table S8). It was found that the value of the atomic charge at E nicely correlates with the electronegativity of the chalcogen (Figure 2A). Moreover, the calculated charge difference between phosphorus and the chalcogen atom ($\Delta q_{(P-E)} = q_P - q_E$) decreases down the group, with a $\Delta q_{(P-E)}$ of 3.09 for oxygen and only 1.61 for tellurium. Accordingly, one should expect a more covalent character for Te and a more ionic character for O.

To further understand this behavior, we have carried out a QTAIM analysis of (^{i}Pr)$_3$P=E (E = O, S, Se, or Te) molecules. It is worth mentioning that atomic charges obtained from the QTAIM analysis are in very good agreement with those coming

Please cite this article in press as: Pérez-Sánchez et al., Isolation of elusive gold-phosphane tellurides: From bonding to σ-hole dynamics, Cell Reports Physical Science (2025), https://doi.org/10.1016/j.xcrp.2025.102717

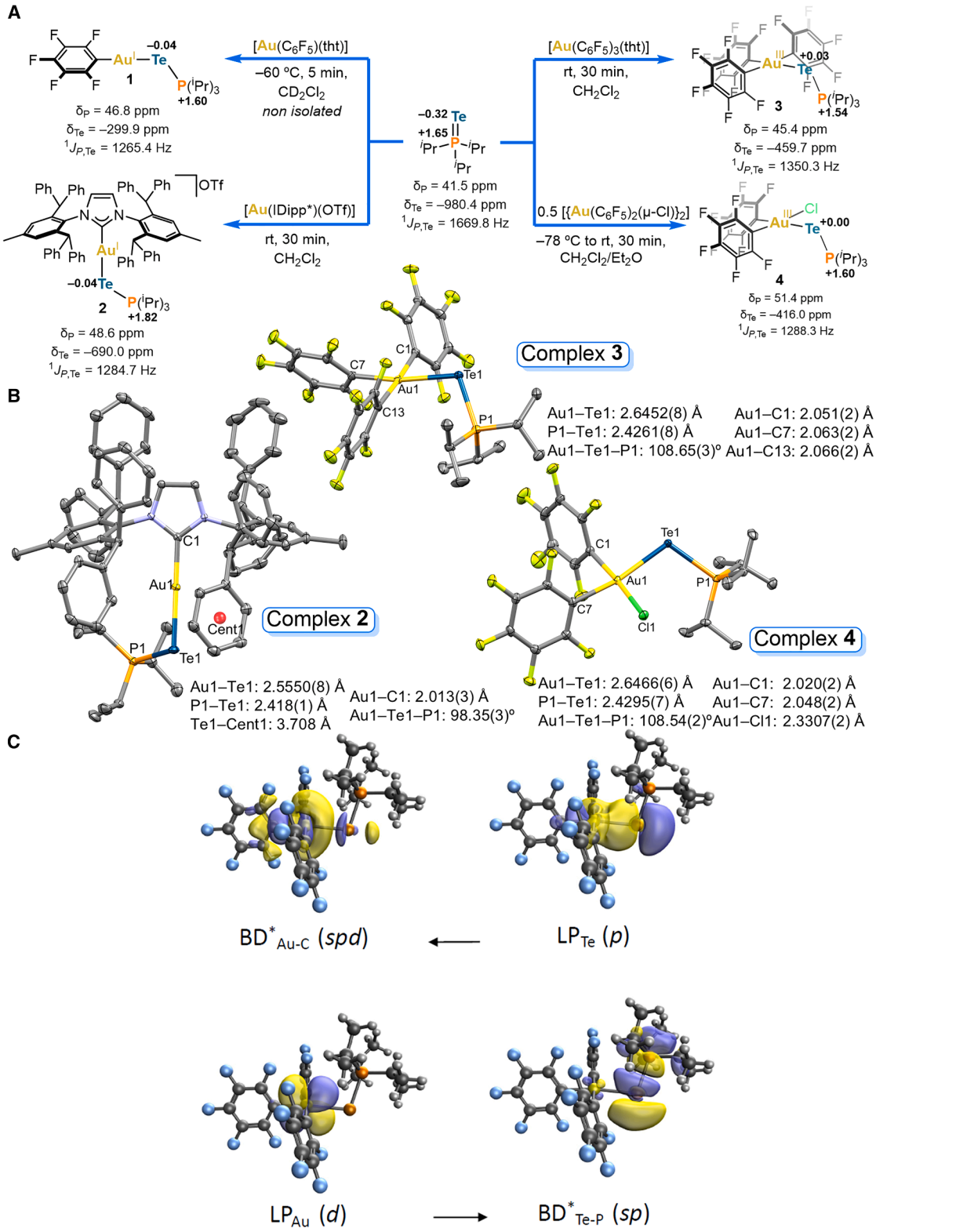

(legend on next page)

Please cite this article in press as: Pérez-Sánchez et al., Isolation of elusive gold-phosphane tellurides: From bonding to σ-hole dynamics, Cell Reports Physical Science (2025), https://doi.org/10.1016/j.xcrp.2025.102717

from the NPA results (Figure 2B). We have also performed a state-of-the-art interacting quantum atoms (IQA) analysis on the nature of the P–E bonds.[7,31–33] This highly demanding decomposition scheme relies on orbital-invariant quantities, such as the reduced first-order density matrix and the pair density, making it independent of any arbitrary reference state. Additionally, it rigorously divides the system's energy into physically meaningful components and allows for the decomposition of interactions between atoms or groups of atoms. The IQA method separates the interaction into a classical term (V_{cl}), which is typically related to the electrostatic (or ionic) contribution, and an exchange-correlation term (V_{xc}), which represents the covalent part of the interaction. Our IQA results show a clear evolution in the ionic contribution to the P–E bond when descending the group, with VCI values of −1,271.35 and −15.32 kcal mol^{-1} for O and Te, respectively. Remarkably, the contribution of the ionic term to the bonding is dictated by the charge difference between E and P with an acceptable linear correlation between V_{cl} and $\Delta q_{(P-E)}$ in both QTAIM and NPA (Figure 2B). We have found notable differences in the nature of the P–E bond, going from mostly ionic bonds in the case of O and S to practically covalent bonds for Se and Te (Figure 2C). In the case of the largest chalcogen, the P–Te bond in (^{i}Pr)$_3$P=Te is 91.2% covalent, according to our IQA analysis. As expected, the electron density at the bond critical point (bcp) associated with the P–E bond, systematically decreases along the chalcogen series (Table S9).

If we look at the Laplacian of the electron density, some interesting results appear. For E = O, the value of $\nabla^2\rho(r)$ is clearly positive, indicating an ionic (or a highly polarized) bond, while for E = S – Te, values of $\nabla^2\rho(r)$ are slightly negative or very close to zero, which is associated with less ionic bonding (Figure 2D). In summary, a detailed understanding of the nature of these ligands could have significant implications for comprehending their coordination behavior with transition metals.

Synthesis and characterization of the complexes

Initially, we reacted [Au(C$_6$F$_5$)(tht)] (tht = tetrahydrothiophene) with an equimolar amount of (^{i}Pr)$_3$PTe at room temperature (Figure 3A). This led to immediate decomposition, evidenced by the rapid formation of elemental tellurium, which was visually observed as a black precipitate. No surface plasmon resonance at 520–530 nm, characteristic of spherical (Ø10–100 nm) Au nanoparticles,[34] was detected in the UV-visible (UV-vis) spectrum (Figure S4). By lowering the reaction temperature to −60°C, a persistent yellow solution was formed, which rapidly decomposed upon warming, yielding [Au(C$_6$F$_5$){P(^{i}Pr)$_3$}] and [Au{(P(^{i}Pr)$_3$}$_2$]$^+$ (Figures S3, S5, and S6). The characterization of complex **1** was thus carried out using multinuclear nuclear magnetic resonance (NMR) at −60°C (Figures S1–S7). In an attempt to stabilize a gold(I) phosphane telluride complex, we next explored other ubiquitous cationic gold(I) complexes of the type [AuL(NCMe)]$^+$ (L = JohnPhos = (2-biphenyl)-di-*tert*-butylphosphane or IDipp = 1,3-bis(2,6-diisopropylphenyl)imidazol-2-ylidene). However, these reactions also resulted in the rapid decomposition of the product, even at low temperatures, with the formation of Te^0. This undesired reactivity was prevented by employing a highly sterically demanding N-heterocyclic carbene (NHC) ligand, such as IDipp* (IDipp* = 1,3-bis(2,6-bis(diphenylmethyl)-4-methylphenyl)imidazol-2-ylidene). Thus, the bulky ligand provided sufficient steric protection to stabilize gold(I) complex **2** at room temperature, both in solution and in the solid state (Figure 3A). In contrast to the other ligands, the use of IDipp* avoided Te^0 formation, as the steric bulk seems to play a key role in stabilizing gold(I) phosphane telluride complexes. As far as we are aware, this marks the first successful isolation of a gold(I) complex featuring a terminal (^{i}Pr)$_3$PTe ligand under ambient conditions without decomposition issues.

Complex **1** exhibits chemical shifts of δ_P = 46.8 ppm (Figure S2) and δ_{Te} = −299.9 ppm (Figure S7), while complex **2** shows δ_P = 48.6 ppm (Figure S8) and δ_{Te} = −690.0 ppm (Figure S11). Both complexes demonstrate a notable downfield shift relative to the free ligand (^{i}Pr)$_3$PTe (δ_P = 41.5 ppm and δ_{Te} = −980.4 ppm). For **1** and **2**, q_{Te} becomes more positive (Δq_{Te} ($|q_{Te,complex} - q_{Te,ligand}|$) = 0.28), as the tellurium atom is electron depleted upon coordination to the gold(I) center (Figure 3A). This effect is more pronounced in **1**, with $\Delta\delta_{Te}$ ($|\delta_{Te,complex} - \delta_{Te,ligand}|$) = 680.5 ppm, compared to $\Delta\delta_{Te}$ = 290.4 ppm in **2**. Likewise, the ^{31}P chemical shifts in both complexes reflect the same trend, as the more downfield δ_P is observed for the phosphorus atom with the higher positive charge. The large difference in ^{125}Te chemical shifts between **1** and **2** may likely arise from the differing electronic environments of the gold(I) centers. The strong electron-withdrawing or electron-donating properties of C$_6$F$_5$ or IDipp* moieties agree with greater and smaller $\Delta\delta_{Te}$ observed for **1** and **2**, respectively.[35] Comparing these values with literature, gold(I) complexes derived from N(Te-P^{i}Pr$_2$)$_2$ show δ_{Te} values of −642[36] and −532.6[37] ppm, which are more negative than those of **1** but closer to **2**, suggesting that the latter retains more phosphane telluride character. Meanwhile, comparisons with gold(I) tellurolates, such as those containing TeC(SiMe$_3$)$_3$, with a δ_{Te} = −148 ppm,[38] implies a trend toward tellurolate-like behavior for **1**. Additionally, **1** displays a $^1J_{P,Te}$ = 1,265.4 Hz, while **2** exhibits $^1J_{P,Te}$ = 1,284.7 Hz. These values are lower than that of free (^{i}Pr)$_3$PTe ($^1J_{P,Te}$ = 1,669.8 Hz), indicating a weakening of the P–Te bond. Notably, **2** shows a more polarized P–Te bond ($\Delta q_{(P-Te)}$ = 1.86) compared to **1** ($\Delta q_{(P-Te)}$ = 1.60), suggesting a more ionic character of the bonding, thus leading to a strengthening of the P–Te bond,[39] as observed in its higher $^1J_{P,Te}$ for **2** (Figure 3A).

Attempts to crystallize complex **1** were unsuccessful due to its thermal instability, but the molecular structure of **2** (Figure 3B) reveals an Au–Te bond length of 2.5550(8) Å and a P–Te bond length of 2.418(1) Å, which is slightly longer than the typical range for free phosphane tellurides (2.35–2.40 Å),[18] indicating some elongation upon metal coordination. The Au–Te bond length in

Figure 3. Synthesis and characterization of gold(I) and gold(III) complexes

(A) Synthesis, selected spectroscopic data (^{31}P{^{1}H}, ^{125}Te chemical shifts, and $^1J_{P,Te}$, in CD_2Cl_2) and QTAIM charge distribution of complexes **2–4**.

(B) X-ray structure of complexes **2–4**. Ellipsoids are drawn at the 50% probability level; hydrogen atoms, solvent molecules, and counterions have been omitted for clarity.

(C) Selected NBOs of **3** involved in charge transfers. rt, room temperature (20°C–25°C); LP, 1-center valence lone pair; BD*, 2-center antibond (σ*).

complex **2** is shorter than those reported for gold(I) complexes presenting {N(TeP^{i}Pr$_2$)$_2$} ligands (2.616–2.639 Å)[36,37] but comparable to those of gold(I) tellurolates (2.566 Å).[38] The Au1–Te1–P1 (98.35(3)°) indicates the presence of two lone pairs at the tellurium atom. Moreover, this atom establishes a short intramolecular contact (Te1–Cent1: 3.708 Å) with one of the phenyl rings of the NHC wingtip (Figure 3B), presumably through a σ-hole interaction, associated with a bond path in the QTAIM analysis (Figure S29).

Next, we explored the reactivity of (^{i}Pr)$_3$PTe with gold(III), a stronger Lewis acid. The initial reaction of (^{i}Pr)$_3$PTe with gold(III) complex [Au(C^N^C)(Cl)] (C^N^C = 2,6-bis(4-(*tert*-butyl)phenyl) pyridine) resulted, again, in tellurium extrusion and the concomitant formation of [Au(C^N^C){P(^{i}Pr)$_3$}]$^+$ (**5**) (Figure S26). Given this result, we decided to increase the steric bulk of the ligands by switching to the Au(C$_6$F$_5$)$_3$ fragment. Reacting (^{i}Pr)$_3$PTe with [Au(C$_6$F$_5$)$_3$(tht)] in equimolar amounts proceeded smoothly at room temperature, yielding complex **3** (Figure 3A). Similarly, the reaction of (^{i}Pr)$_3$PTe with [{Au(C$_6$F$_5$)$_2$(μ-Cl)}$_2$] was explored (Figure 3A). As anticipated, the absence of one bulky C$_6$F$_5$ group reduced the thermal stability of the resulting complex **4**. Consequently, the synthesis was performed at −78°C, though small amounts of Te^0 were observed upon warming to room temperature. Complex **3** presents δ_P = 45.4 ppm (Figure S13), δ_{Te} = −459.7 ppm (Figure S15), and $^1J_{P,Te}$ = 1,350.3 Hz, while **4** displays δ_P = 51.4 ppm (Figure S18), δ_{Te} = −416.0 ppm (Figure S20), and $^1J_{P,Te}$ = 1,288.3 Hz. As observed in the gold(I) analogs, there is a substantial repolarization of the P–Te bond when coordinated to the metal center.

In this case, both Te atoms support a considerably more positive charge (Δq_{Te} = 0.35 and 0.32 for **3** and **4**, respectively) compared to the gold(I) counterparts. The δ_{Te} values for **3** and **4** fall between those measured for **1** and **2**, probably due to the opposing electronic effects of the pentafluorophenyl group, its negative inductive effect, and the strong positive mesomeric effect of the fluorine atoms.[40] As the number of C$_6$F$_5$ groups increases, greater shielding affects the Te atom. Similarly, δ_P values are consistent with those observed in gold(I) complexes **1** and **2**, with the most downfield values corresponding to the most positive charge on the phosphorus atom (q_P = 1.54 and q_P = 1.60 for **3** and **4**, respectively).

Crystals suitable for single crystal X-ray diffraction (SC-XRD) were also obtained for **3** and **4** (Figure 3B). The gold(III) center adopts a square planar environment in both complexes. In **3**, two C$_6$F$_5$ rings are *trans* to each other, while the third is *trans* to the (^{i}Pr)$_3$PTe ligand. In **4**, the C$_6$F$_5$ groups are mutually *cis* and *trans* to one chloride and one (^{i}Pr)$_3$PTe. The Au–Te bond lengths in **3** (2.6452(8) Å) and **4** (2.6466(6) Å) are longer than that observed in **2** (2.5550(8) Å) but similar to reported gold(III) tellurolates (2.59–2.65 Å).[41,42] These longer Au–Te bonds suggest slightly weaker Au–Te interactions in the gold(III) complexes **3** and **4** compared to the gold(I) analogs **1** and **2**, consistent with the softer Pearson acid character of gold(I) relative to gold (III),[43,44] as the former tends to form stronger bonds with soft bases like tellurium. The P–Te bond lengths in **3** (2.4261(8) Å) and **4** (2.4295(7) Å) further support this intermediate bonding behavior, as they are slightly longer than those in free phosphane tellurides (2.35–2.40 Å) and in **2** (2.418(1) Å). Natural bond orbital (NBO) analysis for complex **3** (Figure 3C) reveals that electron donation occurs from a lone pair (p-orbital) with π symmetry on the tellurium atom to the antibonding Au–C spd orbital, accompanied by back donation from the lone pair on the d orbital of gold to the Te–P antibonding sp orbital. The strength of these interactions is markedly different, with the $LP_{Te} \rightarrow BD^*_{Au-C}$ interaction showing a stabilization energy of 147.93 kcal mol^{-1}, while the $LP_{Au} \rightarrow BD^*_{Te-P}$ back donation contributes a far smaller energy of 0.83 kcal mol^{-1} (Table S11). Thus, tellurium acts as the dominant donor of the interaction, whereas the antibonding nature of the Te–P orbital may be less favorable for accepting electron density from the gold center. This bonding framework can also extend to the gold(I) complexes and tentatively provides some hints to their instability, particularly the gold(I) pentafluorophenyl species compared to the gold(III) counterparts. The back donation from Au(I) to the ligand, which populates an antibonding Te–P orbital, likely weakens the Te–P bond, contributing to the instability of these species. Combined with the mechanistic insights discussed later, this analysis points out the delicate interplay between stereoelectronic structure and stability. Hence, when comparing complexes **1**–**4**, some differences can be noted. Gold(I) complexes **1** and **2** exhibit more substantial changes in their ^{125}Te chemical shifts and lower $^1J_{P,Te}$ values, reflecting a weakening of the P–Te bond in the gold(I) species. In contrast, gold(III) complexes **3** and **4** exhibit smaller deshielding and higher $^1J_{P,Te}$ values, indicative of stronger P–Te interactions compared to the gold(I) complexes. Their δ_{Te} values fall between those of gold(I) phosphane tellurides and tellurolates, suggesting a mixed bonding character. Also, the longer Au–Te bond lengths observed in the gold(III) complexes indicate slightly weaker gold–tellurium interactions compared to their gold(I) counterparts. This is in line with the more energetic charge transfer processes from Te lone pair to the gold acceptor orbitals calculated for **1** and **2** with respect to **3** and **4**. Overall, the bonding characteristics in these complexes are significantly influenced by both the stereoelectronic attributes of the ligands and the oxidation state of gold.

σ-hole enhancement and ChB catalysis

The coordination of (^{i}Pr)$_3$PTe to the gold center not only alters its electronic properties but also leads to a notable enhancement of the σ-hole present on the tellurium atom. This phenomenon, characteristic of chalcogens, involves an electron density depletion opposite to the covalent bond, enhancing its electrophilic and interaction capabilities.[9,21,45] Within group 16, tellurium stands out for its stronger chalcogen-bonding ability compared to sulfur and selenium, which is attributed to its higher polarizability and deeper σ-hole. However, its role in ChB catalysis remains limited.

Notable advancements include divalent tellurium-based catalysts bearing electron-withdrawing substituents,[46,47] tetravalent tellurium catalysts,[25,48] and, more recently, a Te(VI) hexavalent ChB catalyst.[49] In our hands, we observed that coordination to gold provides an alternative and efficient strategy for σ-hole modulation. Density functional theory (DFT) calculations performed on complexes **1**–**3** confirmed the presence of a σ-hole along the Te–P bond (Figure 4B). For free (^{i}Pr)$_3$PTe, the electrostatic surface potential (ESP) map shows a V_s value of

Cell Reports
Physical Science
Article

CellPress
OPEN ACCESS

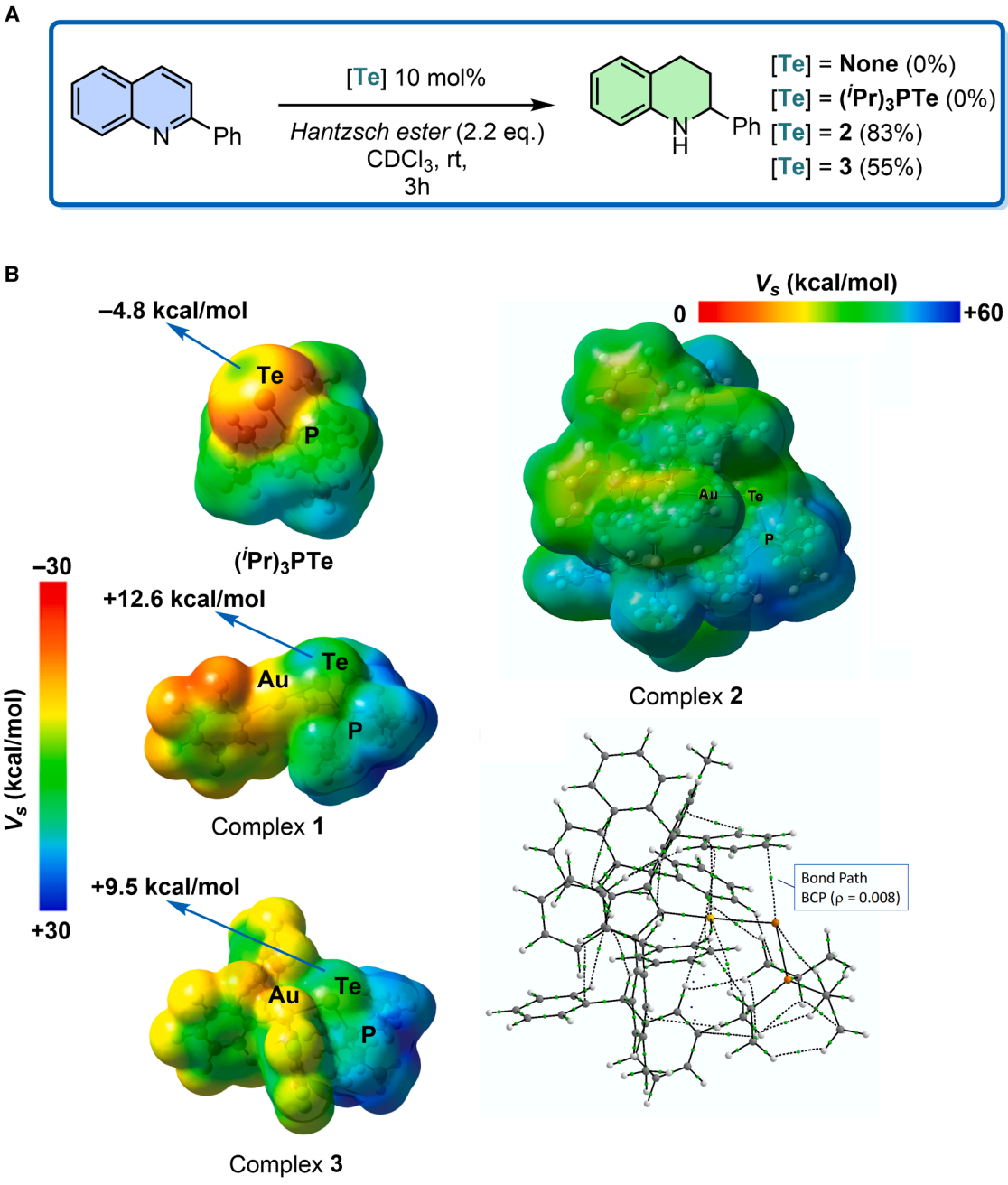

Figure 4. Gold mediated σ-hole enhancement

(A) Transfer hydrogenation of 2-phenylquinoline via chalcogen bond catalysis showing conversion values.

(B) Electrostatic surface potential (ESP) maps for compounds **1**–**3**, (^{i}Pr)$_3$PTe and QTAIM graph of **3**, and value of the electron density at the bond critical point is given in a.u. V_s (kcal/mol), electrostatic potential on the molecular surface.

−4.8 kcal mol^{-1} at the σ-hole region. Upon coordination to gold, the σ-hole depth increases significantly, with a 3.6-fold enhancement observed in **1**. Meanwhile, the most electropositive regions of the molecule are localized on the C–H terminations of the isopropyl groups; pnictogen bonding is effectively suppressed due to the hypervalent character of the phosphorus atom and the steric shielding imposed by the bulky substituents. In contrast, the tellurium atom exhibits a pronounced σ-hole (+12 kcal mol^{-1} in the ESP map) and an accessible σ* orbital, making it a clear electrophilic site susceptible to nucleophilic interactions.

Encouraged by this unique activation mode, we explored the catalytic activity of the complexes on the benchmark hydrogenation of 2-phenylquinoline in the presence of the

Please cite this article in press as: Pérez-Sánchez et al., Isolation of elusive gold-phosphane tellurides: From bonding to σ-hole dynamics, Cell Reports Physical Science (2025), https://doi.org/10.1016/j.xcrp.2025.102717

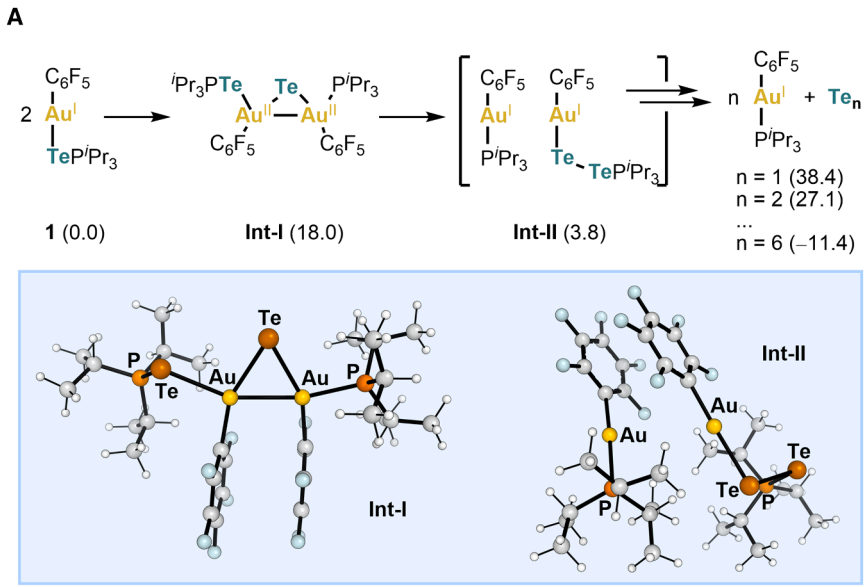

Figure 5. DFT mechanistic studies

(A) Intermediates for Te transfer and formation of Te aggregates.

(B) Stability study of tellurated compounds. G in kcal mol^{-1}. DFT method: ωB97X-D/def2QZVPP// ωB97X-D/def2SVP (solvation model density, SMD, in all calculations). Similar conclusions were obtained when relativistic effects were included in the calculations (Figure S31).

Hantzsch ester (Figure 4A).[50] Complex **2** achieved up to 83% conversion, whereas complex **3** reached only 55% within the same time frame (Figures S27–S29; Table S7). This difference in reactivity directly correlates with the σ-hole magnitude and the increased Lewis acidity of the Te atom, making it a better ChB donor. The superior performance of **2** can be attributed to its cationic nature, which further amplifies the σ-hole effect. In contrast, free $(^{i}Pr)_3PTe$, which has an almost negligible σ-hole, was inactive as the catalyst. Interestingly, in **2**, steric crowding initially shields the σ-hole due to a phenyl ring (Figure 4B). However, the flexibility of the NHC wingtip allows this region to become accessible during the catalytic cycle, facilitating effective substrate activation and reactivity. Complex **3**, in contrast, exhibits slower reaction kinetics, most likely due to its neutral charge and a comparatively weaker σ-hole effect. The thermal instability of **1** prevented its direct evaluation in catalysis, but its V_s value suggests that it could be a highly effective catalyst. Overall, these results demonstrate that metal coordination provides a powerful tool for tuning the σ-hole on tellurium, enabling original modes of activation for ChB catalysis.

Understanding decomposition pathways and Te transfer processes

As previously discussed, some of these gold(I) and gold(III) complexes decompose at room temperature, leading to the rapid formation of Te^0. To understand the underlying reasons for this instability, we initially studied the reactivity of complex **1** using DFT[51–53] since its rapid decomposition at room temperature contrasts with the stability observed for **2**–**4**. Interestingly, **1** can be observed by NMR at −60°C, but this product decomposes rapidly when brought to room temperature to form [Au$(C_6F_5)(P^{i}Pr_3)$] and Te solid nanoparticles aggregates (Figures S3 and S35). These observations suggest that there is a Te transfer side pathway that compromises product stability even at mild temperatures. Multiple unimolecular mechanisms were modeled to understand the Te transfer process using a single molecule of **1** and $(^{i}Pr)_3PTe$. However, in all cases, the energies of intermediate complexes were too high to proceed at room temperature (Figure S30). When including two sets of reagents, the energy required to form systems that could lead to Te transfer drops substantially (18.0 and 3.8 kcal mol^{-1} for **Int-I** and **Int-II**, respectively; Figure 5A). The proposed mechanism (Figure 5A) would involve the aggregation of two molecules of **1**, facilitated by intermolecular Au···Au contacts. This aggregation could drive a 2c-2e (2-center-2-electron) oxidative insertion to form a bimetallic gold(II) complex, **Int-I**, supported by a bridging telluride ligand. While oxidative insertion of tellurium is rare, a few examples have been reported.[34,54] Following this oxidative insertion, the Te^{2-} bridge would then be cleaved via 2c-2e reductive elimination, giving two molecules of Au(I), **Int-II**. These Au(I) species would subsequently evolve through the aggregation of Te atoms, potentially forming Te_n clusters (Figure S35), which would likely act as the driving force for decomposition due to their high relative stability. The species **Int-I** and **Int-II** are transient reaction intermediates that are too short-lived to be detected within a rapid reaction timescale. Thus, multiple molecules of both reagents are

also needed to achieve exergonic Te transfers that could justify the particles observed experimentally (38.4 and −11.4 kcal mol^{-1} for one and six sets, respectively, Te_n; Figure 5A). Overall, all these results suggest that **1** decomposition is a complex mechanism that involves multiple molecules of both reagents. While we did not include any transition state calculations to estimate the kinetics of the process, it is worth noting that, qualitatively, we identified only one thermodynamically feasible pathway based on the energies of the intermediates involved (Figure S30).

The possibility of stabilization of a gold(I) complex with a very bulky carbene prompted us to believe that steric effects governed the interplay of productive and side pathways. Nevertheless, when we tried to expand the experimental product scope with more complexes, we did not observe any clear trend between stability and buried volume (Figures S31–S33). We then compared the energy required for the Te transfer process using the Au(I) and Au(III) synthesized complexes (Figure 5B). In the case of unstable complexes **1** and **5**, favorable self-aggregation is seen (ΔG_1 of −1.8 and −9.7 kcal mol^{-1}), which is in sharp contrast to the significantly unfavorable aggregate of **3** (ΔG_1 of 7.2 kcal mol^{-1}). Similarly, the intermediate that drives the Te transfer process (**Int**) presents very low to favorable energies for the unstable complexes (ΔG_2 of 3.8 and −10.4 kcal mol^{-1} for **1** and **5**, respectively), while this intermediate becomes highly disfavored for the stable product **3** (ΔG_2 of 26.9 kcal mol^{-1}). The barrier observed in **3** is prohibitive for processes occurring at room temperature, thereby preventing access to the decomposition side pathway. These computational results match the experimental outcomes and indicate that both electronic and steric effects control the rate of the decomposition pathway.

The increasing technological relevance of tellurium highlights the necessity of advancing its coordination chemistry, particularly with transition metals like gold. In summary, this study has systematically investigated the synthesis of previously elusive gold(I) and gold(III) phosphane telluride complexes, uncovering key bonding trends, stability factors, and distinctive reactivity patterns. Through successful synthesis and characterization, we have demonstrated the profound influence of electronic and steric effects on their structural and chemical behavior, establishing a foundation for controlled tellurium transfer processes, an essential step toward the rational design of novel materials with tailored electronic and optical properties. Gold(I) complexes exhibited greater reactivity and instability compared to their gold(III) counterparts, most likely due to back donation into antibonding Te–P orbitals, which weakens Te–P bonds. In contrast, gold(III) complexes displayed enhanced stability and stronger P–Te interactions, as revealed by spectroscopic, structural, and bonding analyses. The stabilization of thermally unstable gold(I) species using sterically demanding N-heterocyclic carbene ligands represents a significant breakthrough, enabling the isolation of elusive intermediates and the elucidation of decomposition pathways. Mechanistic studies highlighted the role of Au···Au interactions in facilitating tellurium transfer, with computational analyses reinforcing the critical influence of steric and electronic factors on stability. Theoretical investigations further demonstrated the modulation of the tellurium σ-hole upon coordination with gold, introducing a different perspective on chalcogen bonding catalysis and an original mode of activation. By bridging fundamental inorganic chemistry with the rational design of tellurium-based coordination complexes, this research advances our understanding of metal–tellurium interactions. These findings offer strategies for controlling tellurium transfer processes, expanding the scope of chalcogen-bonding applications, and unlocking pathways for the development of innovative materials and catalytic systems.

METHODS

General considerations

All manipulations were performed under an inert nitrogen atmosphere using standard Schlenk techniques unless stated otherwise. Commercial reagents were used without further purification. Solvents were dried and degassed using standard procedures.

Synthesis of Au(I) and Au(III) complexes

Gold(I) and gold(III) phosphane telluride complexes were synthesized by reacting (^{i}Pr)$_3$PTe[55] with [Au(C_6F_5)(tht)],[56] [AuL(NCMe)][OTf], [Au(C_6F_5)$_3$(tht)],[56] or [{Au(C_6F_5)$_2$(μ-Cl)}$_2$][57] in dichloromethane at low temperatures (typically −78°C to 25°C), depending on the desired complex. Stoichiometry and ligand identity (L) were optimized to avoid decomposition. In particular, bulky NHC ligands such as IDipp* were essential for the stabilization of gold(I) phosphane telluride complex.

Characterization

NMR spectra (^{1}H, ^{31}P{^{1}H}, ^{19}F, and ^{125}Te) were recorded in CD_2Cl_2 on Bruker 300–500 MHz spectrometers. Chemical shifts are reported in ppm and referenced to the residual ^{1}H signal of the deuterated solvent as an internal reference or to external standards (^{31}P{^{1}H}-, ^{19}F-, and ^{125}Te-NMR). Coupling constants (*J*) are given in Hz. X-ray diffraction data for complexes **2**–**5** were collected at low temperatures using MoK α radiation. Structures were solved using SHELXT and refined using SHELXL.[58] ESP maps and QTAIM[28] analyses were derived from optimized DFT geometries.[48–50] Fourier transform infrared (FTIR) spectroscopy spectra in solid-state by attenuated total reflection (ATR) method, positive electrospray ionization high-resolution mass spectrometry (HRMS-ESI+), and elemental analyses were obtained using standard techniques.

Computational details

Geometry optimizations were carried out using DFT at the PBE0-D3(BJ)/def2-TZVP level of theory, including scalar relativistic effects via effective core potentials (ECPs). Charge distributions were evaluated via NPA and QTAIM.[26,28] Bonding interactions were further analyzed by IQA and NBO methods using NBO6 software.[29,30] Transition state searches and decomposition pathway analyses were performed with Gaussian 16,[48] with thermochemical corrections applied using GoodVibes.[50]

ChB catalysis hydrogenation

In a typical experiment, a mixture of 2-phenylquinoline (0.028 mmol) and the gold complex (**2** or **3**, 10 mol %, 0.0028 mmol) was dissolved in $CDCl_3$ (0.5 mL) in a 5 mL scintillation vial. Hantzsch ester (0.06 mmol, 2.2 equiv) was then added, affording

CellPress OPEN ACCESS

Cell Reports Physical Science Article

a pale yellow solution. The reaction mixture was stirred at room temperature for 3 h. Subsequently, the solution was transferred to an NMR tube, and the conversion was determined by integrating characteristic ^{1}H-NMR signals of both the starting material and the product.

Further details regarding the methods can be found in the supplemental information.

RESOURCE AVAILABILITY

Lead contact

Further information and requests for resources and reagents should be directed to and will be fulfilled by the lead contact, M. Concepción Gimeno (gimeno@unizar.es).

Materials availability

Complexes generated in this study will be made available upon reasonable request. For requests with potential commercial applications, a completed material transfer agreement (MTA) and/or cost recovery may be required.

Data and code availability

- All data supporting the findings of this study are available within the paper and its supplemental information. The supplemental information includes detailed experimental and computational procedures.
- This paper does not report original code.
- Any additional information required to reanalyze the data reported in this paper is available from the lead contact upon request.
- CCDC deposition numbers CCDC: 2419504 (**2**), 2419505 (**3**), 2419506 (**4**), and 2419507 (**5**) contain the supplemental crystallographic data. These data can be obtained free of charge by the Cambridge Crystallography Data Center at www.ccdc.cam.ac.uk/structures.

ACKNOWLEDGMENTS

The authors are thankful for projects PID2022-136861NB-I00, PID2022-140159NA-I00, PID2022-140244NB-I00, and PID2023-147471NB-I00 funded by MICIU/AEI/10.13039/501100011033 and Gobierno de Aragón (Research Group E07_23R) for the financial support of their research. J.C.P.-S. also thanks MICIU for a predoctoral grant (FPU21/01888). J.V.A.-R. acknowledges the computing resources at the Galicia Supercomputing Center, CESGA, including access to the FinisTerrae supercomputer, and the Drago cluster facility of SGAI-CSIC. The authors would like to acknowledge the use of Servicio General de Apoyo a la Investigación-SAI, Universidad de Zaragoza, and CSIC. The authors also acknowledge the use of instrumentation as well as the technical advice provided by the National Facility ELECMI ICTS, node Laboratorio de Microscopias Avanzadas (LMA) at Universidad de Zaragoza.

AUTHOR CONTRIBUTIONS

J.C.P.-S. carried out experimental work, including the synthesis and characterization of the complexes, as well as the reactivity studies and catalytic investigations. J.E. and J.V.A.-R. conducted computational studies related to bonding and mechanisms, respectively. M.C.G. and R.P.H. conceptualized the project, supervised the overall work, and wrote the manuscript with the participation of all authors.

DECLARATION OF INTERESTS

The authors declare no competing interests.

SUPPLEMENTAL INFORMATION

Supplemental information can be found online at https://doi.org/10.1016/j.xcrp.2025.102717.

Received: April 11, 2025
Revised: May 9, 2025
Accepted: June 20, 2025

REFERENCES

1. Lin, S., Li, W., Chen, Z., Shen, J., Ge, B., and Pei, Y. (2016). Tellurium as a high-performance elemental thermoelectric. Nat. Commun. *7*, 10287. https://doi.org/10.1038/ncomms10287.
2. Niu, C., Huang, S., Ghosh, N., Tan, P., Wang, M., Wu, W., Xu, X., and Ye, P. D. (2023). Tunable Circular Photogalvanic and Photovoltaic Effect in 2D Tellurium with Different Chirality. Nano Lett. *23*, 3599–3606. https://doi.org/10.1021/acs.nanolett.3c00780.
3. Qiu, G., Charnas, A., Niu, C., Wang, Y., Wu, W., and Ye, P.D. (2022). The resurrection of tellurium as an elemental two-dimensional semiconductor. npj 2D Mater. Appl. *6*, 17. https://doi.org/10.1038/s41699-022-00293-w.
4. Yang, T., Ke, H., Wang, Q., Tang, Y., Deng, Y., Yang, H., Yang, X., Yang, P., Ling, D., Chen, C., et al. (2017). Bifunctional Tellurium Nanodots for Photo-Induced Synergistic Cancer Therapy. ACS Nano *11*, 10012–10024. https://doi.org/10.1021/acsnano.7b04230.
5. Henriquez-Figuereo, A., Morán-Serradilla, C., Angulo-Elizari, E., Sanmartín, C., and Plano, D. (2023). Small molecules containing chalcogen elements (S, Se, Te) as new warhead to fight neglected tropical diseases. Eur. J. Med. Chem. *246*, 115002. https://doi.org/10.1016/j.ejmech.2022.115002.
6. Chivers, T., and Laitinen, R.S. (2015). Tellurium: a maverick among the chalcogens. Chem. Soc. Rev. *44*, 1725–1739. https://doi.org/10.1039/C4CS00434E.
7. Bleiholder, C., Werz, D.B., Köppel, H., and Gleiter, R. (2006). Theoretical Investigations on Chalcogen−Chalcogen Interactions: What Makes These Nonbonded Interactions Bonding? J. Am. Chem. Soc. *128*, 2666–2674. https://doi.org/10.1021/ja056827g.
8. Gleiter, R., Haberhauer, G., Werz, D.B., Rominger, F., and Bleiholder, C. (2018). From Noncovalent Chalcogen–Chalcogen Interactions to Supramolecular Aggregates: Experiments and Calculations. Chem. Rev. *118*, 2010–2041. https://doi.org/10.1021/acs.chemrev.7b00449.
9. Kolb, S., Oliver, G.A., and Werz, D.B. (2020). Chemistry Evolves, Terms Evolve, but Phenomena Do Not Evolve: From Chalcogen–Chalcogen Interactions to Chalcogen Bonding. Angew. Chem. Int. Ed. *59*, 22306–22310. https://doi.org/10.1002/anie.202007314.
10. He, Z., Yang, Y., Liu, J.-W., and Yu, S.-H. (2017). Emerging tellurium nanostructures: controllable synthesis and their applications. Chem. Soc. Rev. *46*, 2732–2753. https://doi.org/10.1039/C7CS00013H.
11. Taylor, M.S. (2020). Anion recognition based on halogen, chalcogen, pnictogen and tetrel bonding. Coord. Chem. Rev. *413*, 213270. https://doi.org/10.1016/j.ccr.2020.213270.
12. Pale, P., and Mamane, V. (2023). Chalcogen Bonding Catalysis: Tellurium, the Last Frontier? Chem. Eur J. *29*, e202302755. https://doi.org/10.1002/chem.202302755.
13. Cremer, C., Goswami, M., Rank, C.K., de Bruin, B., and Patureau, F.W. (2021). Tellurium(II)/Tellurium(III)-Catalyzed Cross-Dehydrogenative C−N Bond Formation. Angew. Chem. Int. Ed. *60*, 6451–6456. https://doi.org/10.1002/anie.202015248.
14. Kuhn, N., Schumann, H., and Wolmershäuser, G. (1985). $M(CO)_5(R_3PTe)$ (M = Cr, Mo, W; R = Bu^t): the first stable tellurophosphorane complexes. J. Chem. Soc. Chem. Commun., 1595–1597. https://doi.org/10.1039/C39850001595.
15. Kuhn, N., and Schumann, H. (1987). Phosphorus–tellurium compounds. Part 3. Cyclopentadienyliron tellurophosphorane complexes: tellurium-bridged iron phosphine compounds? J. Chem. Soc. Dalton Trans., 541–544. https://doi.org/10.1039/DT9870000541.
16. Daniliuc, C., Druckenbrodt, C., Hrib, C.G., Ruthe, F., Blaschette, A., Jones, P.G., and Du Mont, W.-W. (2007). The first trialkylphosphane telluride complexes of Ag(I): molecular, ionic and supramolecular structural

alternatives. Chem. Commun. *2060*, 2060–2062. https://doi.org/10.1039/b700917h.

17. Pérez-Sánchez, J.C., Ceamanos, C., Herrera, R.P., and Gimeno, M.C. (2023). Unravelling the role of triisopropylphosphane telluride in Ag(I) complexes. Inorg. Chem. Front. *10*, 6519–6525. https://doi.org/10.1039/D3QI01485A.
18. Nordheider, A., Woollins, J.D., and Chivers, T. (2015). Organophosphorus-Tellurium Chemistry: From Fundamentals to Applications. Chem. Rev. *115*, 10378–10406. https://doi.org/10.1021/acs.chemrev.5b00279.
19. Gimeno, M.C. (2007). Handbook of Chalcogen Chemistry New Perspectives in Sulfur, Selenium and Tellurium, Volume 2. In Handbook of Chalcogen Chemistry New Perspectives in Sulfur, Selenium and Tellurium, *2*, F. Devillanova and W.W. Du Mont, eds. (Royal Society of Chemistry), pp. 37–94. https://doi.org/10.1039/9781847557575.
20. L.J. Higham, D.W. Allen, and J.C. Tebby, eds. (2022). Organophosphorus Chemistry (Royal Society of Chemistry). https://doi.org/10.1039/9781839166198.
21. Vogel, L., Wonner, P., and Huber, S.M. (2019). Chalcogen Bonding: An Overview. Angew. Chem. Int. Ed. *58*, 1880–1891. https://doi.org/10.1002/anie.201809432.
22. Durrant, M.C. (2015). A quantitative definition of hypervalency. Chem. Sci. *6*, 6614–6623. https://doi.org/10.1039/C5SC02076J.
23. Walther, B. (1984). The coordination chemistry of secondary phosphine chalcogenides and their conjugate bases. Coord. Chem. Rev. *60*, 67–105. https://doi.org/10.1016/0010-8545(84)85062-6.
24. Keglevich, G. (2024). Phosphine chalcogenides. In Organophosphorus Chemistry, L.J. Higham and D.W. Allen, eds. (Royal Society of Chemistry), pp. 26–57. https://doi.org/10.1039/BK9781837672738-00026.
25. Zhou, B., and Gabbaï, F.P. (2021). Anion Chelation via Double Chalcogen Bonding: The Case of a Bis-telluronium Dication and Its Application in Electrophilic Catalysis via Metal–Chloride Bond Activation. J. Am. Chem. Soc. *143*, 8625–8630. https://doi.org/10.1021/jacs.1c04482.
26. Wang, Q.-M., Lee, Y.-A., Crespo, O., Deaton, J., Tang, C., Gysling, H.J., Concepción Gimeno, M., Larraz, C., Villacampa, M.D., Laguna, A., and Eisenberg, R. (2004). Intensely Luminescent Gold(I)−Silver(I) Cluster Complexes with Tunable Structural Features. J. Am. Chem. Soc. *126*, 9488–9489. https://doi.org/10.1021/ja048091d.
27. Srinivasa Reddy, T., Privér, S.H., Mirzadeh, N., Luwor, R.B., Ganga Reddy, V., Ramesan, S., and Bhargava, S.K. (2020). Antitumor and Antiangiogenic Properties of Gold(III) Complexes Containing Cycloaurated Triphenylphosphine Sulfide Ligands. Inorg. Chem. *59*, 5662–5673. https://doi.org/10.1021/acs.inorgchem.0c00423.
28. Streltsov, S.V., Roizen, V.V., Ushakov, A.V., Oganov, A.R., and Khomskii, D. I. (2018). Old puzzle of incommensurate crystal structure of calaverite $AuTe_2$ and predicted stability of novel AuTe compound. Proc. Natl. Acad. Sci. USA *115*, 9945–9950. https://doi.org/10.1073/pnas.1802836115.
29. Reed, A.E., Weinstock, R.B., and Weinhold, F. (1985). Natural population analysis. J. Chem. Phys. *83*, 735–746. https://doi.org/10.1063/1.449486.
30. Bader, R.F.W. (1990). Atoms in Molecules: A Quantum Theory (Clarendon press).
31. Blanco, M.A., Martín Pendás, A., and Francisco, E. (2005). Interacting Quantum Atoms: A Correlated Energy Decomposition Scheme Based on the Quantum Theory of Atoms in Molecules. J. Chem. Theor. Comput. *1*, 1096–1109. https://doi.org/10.1021/ct0501093.
32. Pendás, A.M., Blanco, M.A., and Francisco, E. (2007). Chemical fragments in real space: Definitions, properties, and energetic decompositions. J. Comput. Chem. *28*, 161–184. https://doi.org/10.1002/jcc.20469.
33. Haberhauer, G., and Gleiter, R. (2020). The Nature of Strong Chalcogen Bonds Involving Chalcogen-Containing Heterocycles. Angew. Chem. Int. Ed. *59*, 21236–21243. https://doi.org/10.1002/anie.202010309.
34. Perrault, S.D., and Chan, W.C.W. (2009). Synthesis and Surface Modification of Highly Monodispersed, Spherical Gold Nanoparticles of 50−200 nm. J. Am. Chem. Soc. *131*, 17042–17043. https://doi.org/10.1021/ja907069u.
35. Pietrasiak, E., Gordon, C.P., Copéret, C., and Togni, A. (2020). Understanding ^{125}Te NMR chemical shifts in disymmetric organo-telluride compounds from natural chemical shift analysis. Phys. Chem. Chem. Phys. *22*, 2319–2326. https://doi.org/10.1039/C9CP05934B.
36. Copsey, M.C., Panneerselvam, A., Afzaal, M., Chivers, T., and O'Brien, P. (2007). Syntheses, X-ray structures and AACVD studies of group 11 ditelluroimidodiphosphinate complexes. Dalton Trans., 1528–1538. https://doi.org/10.1039/b617429a.
37. Ritch, J.S., and Chivers, T. (2009). Group 11 complexes of the P,Te-centered ligand $[TePiPr_2NPiPr_2]^-$: synthesis, structures, and insertion reactions of the copper(I) complex with chalcogens. Inorg. Chem. *48*, 3857–3865. https://doi.org/10.1021/ic802428b.
38. Bonasia, P.J., Gindelberger, D.E., and Arnold, J. (1993). Synthesis and characterization of gold(I) thiolates, selenolates, and tellurolates: x-ray crystal structures of $Au_4[TeC(SiMe_3)_3]_4$, $Au_4[SC(SiMe_3)_3]_4$, and $Ph_3PAu[TeC(SiMe_3)_3]$. Inorg. Chem. *32*, 5126–5131. https://doi.org/10.1021/ic00075a031.
39. Alvarado, S.R., Shortt, I.A., Fan, H.J., and Vela, J. (2015). Assessing Phosphine-Chalcogen Bond Energetics from Calculations. Organometallics *34*, 4023–4031. https://doi.org/10.1021/acs.organomet.5b00428.
40. Ashley, A.E., Herrington, T.J., Wildgoose, G.G., Zaher, H., Thompson, A.L., Rees, N.H., Krämer, T., and O'Hare, D. (2011). Separating Electrophilicity and Lewis Acidity: The Synthesis, Characterization, and Electrochemistry of the Electron Deficient *Tris* (aryl)boranes $B(C_6F_5)_{3-n}(C_6Cl_5)_n$ (n = 1–3). J. Am. Chem. Soc. *133*, 14727–14740. https://doi.org/10.1021/ja205037t.
41. Eisler, D.J., Robertson, S.D., and Chivers, T. (2009). Gold complexes of ditelluridoimidodiphosphinate ligands — Reversible oxidation of Au(I) to Au(III) via insertion of gold into a phosphorus–tellurium bond. Can. J. Chem. *87*, 39–46. https://doi.org/10.1139/v08-074.
42. Molter, A., and Mohr, F. (2010). Gold complexes containing organoselenium and organotellurium ligands. Coord. Chem. Rev. *254*, 19–45. https://doi.org/10.1016/j.ccr.2009.09.017.
43. Pearson, R.G. (1963). Hard and Soft Acids and Bases. J. Am. Chem. Soc. *85*, 3533–3539. https://doi.org/10.1021/ja00905a001.
44. Skipper, H.E., May, C.V., Rheingold, A.L., Doerrer, L.H., and Kamenetska, M. (2021). Hard–Soft Chemistry Design Principles for Predictive Assembly of Single Molecule-Metal Junctions. J. Am. Chem. Soc. *143*, 16439–16447. https://doi.org/10.1021/jacs.1c05142.
45. Aakeroy, C.B., Bryce, D.L., Desiraju, G.R., Frontera, A., Legon, A.C., Nicotra, F., Rissanen, K., Scheiner, S., Terraneo, G., Metrangolo, P., and Resnati, G. (2019). Definition of the chalcogen bond (IUPAC Recommendations 2019). Pure Appl. Chem. *91*, 1889–1892. https://doi.org/10.1515/pac-2018-0713.
46. Benz, S., Poblador-Bahamonde, A.I., Low-Ders, N., and Matile, S. (2018). Catalysis with Pnictogen, Chalcogen, and Halogen Bonds. Angew. Chem. Int. Ed. *57*, 5408–5412. https://doi.org/10.1002/anie.201801452.
47. Wonner, P., Dreger, A., Vogel, L., Engelage, E., and Huber, S.M. (2019). Chalcogen Bonding Catalysis of a Nitro-Michael Reaction. Angew. Chem. Int. Ed. *58*, 16923–16927. https://doi.org/10.1002/anie.201910639.
48. Weiss, R., Aubert, E., Pale, P., and Mamane, V. (2021). Chalcogen-Bonding Catalysis with Telluronium Cations. Angew. Chem. Int. Ed. *60*, 19281–19286. https://doi.org/10.1002/anie.202105482.
49. Li, X., Liu, Y., Wang, W., and Wang, Y. (2025). A Hexavalent Tellurium-Based Chalcogen Bonding Catalysis Platform: High Catalytic Activity and Controlling of Selectivity. J. Am. Chem. Soc. *147*, 3233–3242. https://doi.org/10.1021/jacs.4c13004.
50. Zhou, B., and Gabbaï, F.P. (2021). Lewis Acidic Telluronium Cations: Enhanced Chalcogen-Bond Donor Properties and Application to Transfer Hydrogenation Catalysis. Organometallics *40*, 2371–2374. https://doi.org/10.1021/acs.organomet.1c00279.

51. Frisch, M.J., Trucks, G.W., Schlegel, H.B., Scuseria, G.E., Robb, M.A., Cheeseman, J.R., Scalmani, G., Barone, V., Petersson, G.A., Nakatsuji, H., et al. (2016). Gaussian 16, Revision C.01. Gaussian, Inc.: Wallingford CT.

52. Alegre-Requena, J.V., Sowndarya, S.V.,S., Pérez-Soto, R., Alturaifi, T.M., and Paton, R.S. (2023). AQME: Automated quantum mechanical environments for researchers and educators. WIREs Comput. Mol. Sci. *13*, e1663. https://doi.org/10.1002/wcms.1663.

53. Luchini, G., Alegre-Requena, J.V., Funes-Ardoiz, I., and Paton, R.S. (2020). GoodVibes: automated thermochemistry for heterogeneous computational chemistry data. F1000Res. *9*, 291. https://doi.org/10.12688/f1000research.22758.1.

54. Martynov, A.V. (2024). Elemental tellurium in organoelement synthesis of tellurium-containing organometallics and telluracycles. J. Organomet. Chem. *1022*, 123418. https://doi.org/10.1016/j.jorganchem.2024.123418.

55. Kuhn, N., Henkel, G., Schumann, H., and Fröhlich, R. (1990). Die Bindungsverhältnisse in Phosphantelluriden. Eine empirische NMR-Studie und die Kristallstruktur von (iso-C_3H_7)$_3$PTe [1]/The Nature of the Bonding in Phosphane Tellurides. An Empirical NMR Study and the Crystal Structure of (iso-C_3H_7)$_3$PTe. Z. Naturforsch. B Chem. Sci. *45*, 1010–1018. https://doi.org/10.1515/znb-1990-0717.

56. Uson, R., Laguna, A., Laguna, M., Briggs, D.A., Murray, H.H., and Fackler, J.P. (1989). (Tetrahydrothiophene)Gold(I) or Gold(III) Complexes. Inorg. Synth. *26*, 85–91. https://doi.org/10.1002/9780470132579.ch17.

57. Usón, R., Laguna, A., Laguna, M., and Abad, M. (1983). Synthesis and reactions of di-μ-halo- or -pseudohalotetrakis(pentafluorophenyl)digold(III). J. Organomet. Chem. *249*, 437–443. https://doi.org/10.1016/S0022-328X(00)99441-5.

58. Sheldrick, G.M. (2015). Crystal structure refinement with SHELXL. Acta Crystallogr. C *71*, 3–8. https://doi.org/10.1107/S2053229614024218.